# Synergistic substrate cofeeding stimulates reductive metabolism

# Synergistic substrate cofeeding stimulates reductive metabolism

Junyoung O. Park[1†], Nian Liu[1†], Kara M. Holinski[1], David F. Emerson[1], Kangjian Qiao[1], Benjamin M. Woolston[1], Jingyang Xu[1], Zbigniew Lazar[1,2], M. Ahsanul Islam[1], Charles Vidoudez[3], Peter R. Girguis[3], and Gregory Stephanopoulos[1*]

[1] Department of Chemical Engineering, Massachusetts Institute of Technology, 77 Massachusetts Avenue, Cambridge, MA 02139

[2] Department of Biotechnology and Food Microbiology, Wroclaw University of Environmental and Life Sciences, Chelmonskiego 37, 51-630, Wroclaw, Poland

[3] Department of Organismic and Evolutionary Biology, Harvard University, 16 Divinity Avenue, Cambridge, MA 02138

[†] Equal contribution

* Correspondence to G.S.: gregstep@mit.edu

Advanced bioproduct synthesis via reductive metabolism requires coordinating carbons, ATP, and reducing agents, which are generated with varying efficiencies depending on metabolic pathways. Substrate mixtures with shortcut access concurrently to multiple pathways may optimally satisfy these biosynthetic requirements. However, native regulation favoring preferential utilization precludes cells from co-metabolizing multiple substrates. Here we explore mixed substrate metabolism and tailor pathway usage to synergistically stimulate carbon reduction. By controlled cofeeding of superior ATP- and NADPH-generators as "dopant" substrates to cells primarily utilizing inferior substrates, we circumvent catabolite repression and drive synergy in two divergent organisms. Glucose doping in *Moorella thermoacetica* stimulates $CO_2$ reduction (2.3 $g/g_{cell}/hr$) into acetate by augmenting ATP synthesis via pyruvate kinase. Gluconate doping in *Yarrowia lipolytica* accelerates acetate-driven lipogenesis (0.046 $g/g_{cell}/hr$) by obligatory NADPH synthesis through the pentose cycle. Together, synergistic cofeeding produces $CO_2$-derived lipids with 38% energetic efficiency and demonstrates potential to convert $CO_2$ into advanced bioproducts.

## Introduction

One of the greatest feats of metabolism is the ability to synthesize reduced compounds from input substrates with varying oxidation states. Using reductive metabolism, cells reassemble the output of substrate catabolism for energy-dense bioproduct synthesis[1]. This process is often implemented in both laboratory and industry with single organic carbon sources (e.g., sugars) as inputs due to simplicity[2,3]. Nonetheless, single substrates naturally impose stoichiometric constraints on available carbons, energy, and redox cofactors, leading to biosynthetic imbalance and suboptimal product yield. Thus, genetic rewiring of metabolic pathways is required to advantageously shift these stoichiometries[4], which precludes wide application of non-model organisms that lack suitable genetic tools[5].

Substrate mixtures, on the other hand, present the potential to alleviate such stoichiometric constraints in reductive metabolism without genetic rewiring. Since each substrate has unique efficiencies for carbon, energy, and cofactor generation, varying the relative amounts of substrates in the mixture allows fine-tuning of carbon-to-energy-to-cofactor ratios. Furthermore, substrates with different entry points to metabolism alleviate protein burdens by providing the required components in fewer enzymatic steps. Nevertheless, mixed substrate metabolism is epitomized by sequential (e.g., diauxie) and hierarchical (yet simultaneous) utilization based on substrate preference[6-8], reflecting the evolutionary fitness of cells in their native environments[9]. Despite the recent success of substrate mixture batch fermentation using limited substrate pairs (that do not trigger catabolite repression)[10,11], genetic engineering[12,13], and directed evolution[14-16], the full mixture spectrum remains inaccessible and thus unexplored.

Here we report a simple and universal solution to overcoming undesirable substrate preferences and improving carbon reduction in various organisms. We eliminate catabolite repression by controlling the continuous feed rate of preferred superior substrates to maintain negligible concentrations in systems dominated by inferior substrates. Using this method, we explored mixed substrate metabolism and therein observed enhanced metabolic productivity that exceeds the sum of individual-substrate productivities.

This substrate cofeeding scheme was applied to two widely divergent organisms to optimize reductive metabolism of lipogenesis and acetogenesis. We cultured the oleaginous yeast *Y. lipolytica* on acetate and continuously fed limiting quantities of glucose, fructose, glycerol, or gluconate as "dopant substrates" to augment reductive metabolism. In this fed-batch setup, cells simultaneously consumed acetate and the supplemented substrate with acetate remaining as the primary carbon source. In particular, the rate of lipogenesis with gluconate doping was twice as fast as that of the acetate-only control. Tracing $^{13}C$ from gluconate revealed that obligatory NADPH synthesis by recursive use of the oxidative pentose phosphate pathway (oxPPP) was responsible for the observed synergy with acetate.

We then set out to source acetate via acetogenesis, a reductive metabolic process starting from $CO_2$. Acetogenic bacterium *M. thermoacetica* simultaneously consumes $CO_2$ and glucose with the latter providing both ATP and electrons ($e^-$) necessary for $CO_2$ fixation, cell maintenance, and growth[17]. However, tracing $^{13}C$-labeled glucose revealed that glucose metabolism dominated and $e^-$ generation was coupled to undesirable decarboxylation. To shift cellular metabolism towards

greater $CO_2$ incorporation, we designed a chemostat that continuously supplied limiting glucose and ample $H_2$. Under these conditions, $CO_2$ reduction metabolism dominated, glucose primarily produced ATP sufficient for cell maintenance via pyruvate kinase, and carbon-free $e^-$ for net $CO_2$ reduction was supplied by $H_2$. Importantly, with dopant substrate glucose, *M. thermoacetica* rapidly converted $CO_2$ into acetate exclusively, serving as the ideal input for gluconate-doped lipogenesis.

With the aforementioned synergy, we fixed $CO_2$ at 2.3 g per g cell dry weight per hour (g $gCDW^{-1}$ $hr^{-1}$), substantially faster than ~0.05 g $gCDW^{-1}$ $hr^{-1}$ of typical photosynthetic systems[18]. Using the resulting acetate, we produced lipids at 0.046 g $gCDW^{-1}$ $hr^{-1}$, a more than two-fold improvement over the previously optimized system (~0.02 g $gCDW^{-1}$ $hr^{-1}$)[19]. Coordinating the glucose-doped acetogenesis and gluconate-doped lipogenesis, we converted carbons in the most oxidized, undesirable state ($CO_2$) to the reduced, energy-dense state (lipids) with 38% energetic efficiency. Through substrate cofeeding, we overcame the limitation of ATP- and NADPH-dependent biological carbon reduction, paving the path for $CO_2$-derived advanced bioproduct synthesis.

**Accelerating lipogenesis from acetate by enhancing NADPH generation in *Y. lipolytica***

Lipogenesis requires a balanced supply of acetyl-CoA, ATP, and NADPH at a ~1:1:2 ratio. Single substrates, such as glucose and acetate, can provide all three building blocks for lipids[19-21]. However, lipid synthesis from acetate, despite acetate's direct contribution to acetyl-CoA and ATP, is slower compared to that from glucose[22] (**Fig. 1A**). This is because in *Y. lipolytica*, NADPH generation is mainly through oxPPP, which takes a series of ATP-intensive reactions to arrive at starting from acetate[23].

We aimed to enhance acetate-to-lipid conversion by better supplying NADPH. Since glucose can flow more directly into oxPPP than acetate, we provided both acetate and glucose to a *Y. lipolytica* batch culture. Consistent with the widely accepted phenomenon of catabolite repression[24], cells consumed glucose only at first (**Supplementary Fig. 1**). To overcome this selective preference (i.e., diauxie), we devised a fed-batch system, in which the same amount of glucose was instead continuously supplied over the course of fermentation to an acetate culture (**Fig. 1B**). The feed rate was kept slow to maintain negligible glucose concentrations in the reactor. In this setup, despite constant introduction of glucose, we observed steadily decreasing acetate and no glucose in the reactor, suggesting simultaneous consumption of the two carbon sources (**Fig. 1C**). Furthermore, the fed-batch cofeeding strategy enhanced both the growth and lipid production in *Y. lipolytica* significantly compared to the acetate-only control (**Fig. 1D,E**).

Using the same fed-batch system, we also tested supplementing other substrates (fructose, glycerol, and gluconate) that enter metabolism near oxPPP as metabolic "dopants" to provide NADPH (**Fig. 2A**). In all cases, we observed simultaneous consumption of acetate and the supplemented substrate (**Supplementary Fig. 2**). As with glucose, cell growth and lipid production were enhanced (**Supplementary Fig. 3**) despite the supplemental substrates constituting only small fractions of carbons (**Fig. 2B**). To distinguish whether the increase in lipid production was due to cellular metabolism enhancements or simply having more cells in the culture, we determined specific growth rates and productivities. Substrate doping nearly doubled both the specific growth rate (**Fig. 2C**) and the specific lipid productivity during nitrogen-replete growth phase (**Fig. 2D**). In nitrogen-depleted lipogenic phase, glucose, fructose, and glycerol cofeeding only modestly

enhanced specific productivity while gluconate cofeeding significantly outperformed all other conditions (**Fig. 2E**).

## Recursive NADPH generation via the pentose cycle

To understand the mechanism of accelerated lipid production, we aimed to elucidate how continuous gluconate supplementation rewires metabolism. Tracing the carbons from [U-$^{13}C_6$]gluconate by liquid chromatography-mass spectrometry (LC-MS), we observed that the $^{13}C$ atoms were confined to the PPP and upper glycolysis (**Fig. 3A and Supplementary Table 1**). Gluconate enters metabolism as 6-phosphogluconate (6PG), which can only go in the oxidative direction through oxPPP because the combined thermodynamics of glucose-6-phosphate dehydrogenase and 6-phosphogluconolactonase ($\Delta G°' = -29$ kJ/mol) strongly favors the flow of 6PG further into PPP[25]. This causes gluconate to obligatorily generate NADPH via 6PG dehydrogenase, which is likely responsible for the acceleration of lipogenesis. On the other hand, metabolites in the TCA cycle as well as fatty acids were completely unlabeled, indicating exclusive contribution of lipogenic acetyl-CoA and ATP from acetate (**Fig. 3A and Supplementary Table 1**). These labeling data suggested the partitioned usage of metabolism where acetate primarily provided acetyl-CoA and ATP while gluconate primarily provided NADPH to meet the metabolic demands of lipogenesis.

To further validate the hypothesis that gluconate enhances lipogenesis through NADPH supplementation, we performed metabolic flux analysis using the labeling data, substrate uptake rates, and lipid production rate. The flux distribution that best fit all these measurements revealed a strong flux through the oxPPP NADPH-generating steps (**Fig. 3B and Supplementary Table 2**). Interestingly, phosphoglucose isomerase operated in the reverse direction converting fructose-6-phosphate (F6P) to glucose-6-phosphate (G6P). The flux analysis also revealed that gluconeogenic, oxPPP, and non-oxPPP fluxes together form a metabolic cycle, which we termed the "pentose cycle" (**Fig. 3B and Supplementary Table 2**). Akin to the TCA cycle, the pentose cycle recursively oxidized the carbons from gluconate into $CO_2$ while preserving the electrons as NADPH for lipogenesis, maximizing the dopant substrate's role as a NADPH provider.

## Preferential use of glucose leads to excessive decarboxylation in $CO_2$-fixing *M. thermoacetica*

Acetogenesis is a reductive metabolic process that produces acetate from $CO_2$. In acetogenic organisms, the reductive acetyl-CoA pathway incorporates $CO_2$ as carbonyl and methyl components of the acetyl group[26] (**Fig. 4A**). The methyl branch of this pathway requires ATP, which acetogens may recover by acetate production. This ATP conservation contributes to efficient autotrophic $CO_2$ fixation[27], but autotrophic culture conditions, which derive energy solely from inorganic sources (e.g., oxidation of $H_2$), results in slow metabolism and low culture density[28,29].

Since glycolysis effectively produces ATP and $e^-$ necessary for operating the reductive acetyl-CoA pathway, we co-fed $CO_2$ and [U-$^{13}C_6$]glucose to *M. thermoacetica* and looked for signs of $CO_2$ incorporation. If acetate were the only product, we would expect up to 100% carbon yield, that is, three acetate molecules per glucose[29]. On the other hand, with potential other products (e.g., pyruvate) or biomass components (e.g., Ser/Gly, Asp, and Glu), net $CO_2$ utilization becomes feasible as some pathways generate reducing agents without $CO_2$ production or fix more $CO_2$ than the amount produced (**Supplementary Fig. 4**). Since net $CO_2$ utilization depends on the types and

fractions of fermentation products, we quantified the cell growth, the secreted molecules, and their carbon yields relative to glucose consumption (**Fig. 4B**). We observed the activity of the reductive acetyl-CoA pathway as the produced acetate accounted for 77% of glucose carbons, exceeding what is possible via glycolysis (67%). However, as glucose carbon consumption rate approximately matched the total carbon output rate of major products (i.e., biomass, acetate, and formate accounted for 93%), we did not observe net $CO_2$ utilization.

We hypothesized that our observed carbon yield was due to insufficient reducing agents available for new $CO_2$ utilization and cells preferentially consuming glucose over $CO_2$. To trace the fate of $^{13}C$-glucose carbons and to visualize metabolic pathway usage, we measured $^{13}C$ enrichment in cellular metabolites using LC-MS. Unlabeled $CO_2$ was provided in the headspace and $CO_2$ remained mostly unlabeled (**Supplementary Fig. 5**). The carbons of glycolytic intermediates were ≥90% labeled except for pyruvate, which was ~50% labeled (**Fig. 4C**, **Supplementary Table 3**). The lower labeling in pyruvate was due to reversible pyruvate:ferredoxin oxidoreductase (PFOR), which can form pyruvate by combining unlabeled $CO_2$ and acetyl group derived from the reductive acetyl-CoA pathway. With phosphoenolpyruvate (PEP) remaining mostly labeled, the contrasting pyruvate labeling indicated that pyruvate kinase (PEP + ADP → Pyr + ATP) was forward-driven to produce ATP.

Interestingly, serine, glycine, as well as other amino acids derived from pyruvate and TCA cycle intermediates were also half-labeled (**Fig. 4C**, **Supplementary Table 3**). These labeling data suggested shared usage of central metabolism, where glucose and $CO_2$ jointly contributed to the TCA cycle (and thus non-aromatic amino acid biosynthesis). However, because glycolysis and the pentose phosphate pathway (and thus the synthesis of nucleotide ribose rings and aromatic amino acids) were driven mainly by glucose, cells incorporated more carbons from glucose. Therefore, despite the simultaneous consumption of $CO_2$ and glucose, lack of observable net $CO_2$ fixation was the result of cells prioritizing ATP production (and cell growth). Prioritizing ATP production involves faster glycolysis via faster glucose uptake. This substrate hierarchy favoring glucose subsequently led to excessive pyruvate decarboxylation via PFOR (**Fig. 4D**, **Supplementary Table 4**) which, together with $CO_2$-producing biosynthetic pathways (**Supplementary Fig. 6**), outpaced $CO_2$ incorporation.

## Accelerating acetate production from $CO_2$ by decoupling $e^-$ supply from decarboxylation

Since undesirable decarboxylation is coupled to the PFOR step for $e^-$ generation from glucose, we aimed to limit the function of glucose as an $e^-$ source and to stimulate net $CO_2$ incorporation. On the other hand, sufficient ATP is still required from glucose through pyruvate kinase to avoid slow metabolism and sustain $CO_2$ reduction. We note that acetate production via the reductive acetyl-CoA pathway does not consume ATP leading to cell maintenance (e.g., housekeeping) being the only ATP requirement for converting $CO_2$ to acetate (**Supplementary Fig. 7**). Hence, we implemented glucose-limiting culture environments in a chemostat to reduce the rate of glycolysis such that it supplies the required ATP but overall decarboxylation is slowed (**Fig. 5A**). To compensate for the decreased $e^-$ availability, cells were provided with $H_2$ as a carbon-free $e^-$ source that yields reducing agents without $CO_2$ generation. In addition, low dilution rates (0.009 and 0.017 $hr^{-1}$) were selected to minimize biomass formation and maximize cell residence time in the reactor.

Using this glucose doping system, productivities and yields at various fractions of electrons derived from glucose versus $H_2$ were obtained (**Fig. 5B**). In this plot, we also included batch results with or without $H_2$ in the headspace (**Supplementary Table 5**). Interestingly, the presence of $H_2$ decreased glucose consumption rate, shifting carbon substrate preferences towards $CO_2$ (**Supplementary Fig. 8**). At steady state, acetate concentration in the effluent from the chemostat could exceed 13 g/L. With decreasing fractions of electrons from glucose, acetate production rate could be more than 80 times as fast as the glucose feed rate, and the carbon yield monotonically increased to >80 g acetate produced per g glucose consumed. This high yield indicated that the overwhelming majority of acetate and biomass was derived from $CO_2$ rather than glucose. While cell growth rates were slow in the chemostat (growth rate = dilution rate), acetate production remained fast (**Fig. 5B**). Importantly, we found that, at 2% of $e^-$ from glucose, glucose doping simultaneously enabled a very high yield (>50 g acetate/g glucose) and a substantial acetate productivity (>9 mmol $gCDW^{-1}$ $hr^{-1}$, ~⅓ of the maximum observed productivity).

Across the glucose+$H_2$ energy landscape, $CO_2$ fixation rates peaked at 52.7 mmol $gCDW^{-1}$ $hr^{-1}$ (2.3 g $gCDW^{-1}$ $hr^{-1}$) (**Fig. 5C**). Such high rates implied that we not only decreased $CO_2$ generation from pyruvate decarboxylation but also increased the reductive acetyl-CoA pathway flux. Furthermore, the maximum rate occurring between the two extremes (glucose-only and $H_2$-only) demonstrated that $CO_2$ fixation rate is determined by a balance between reducing agents and ATP supplied via $H_2$ and glucose, respectively. Thus, by controlled glucose doping, we decoupled $e^-$ supply from decarboxylation, shifted cellular metabolism towards favoring $CO_2$ utilization over glucose, and achieved rapid and continuous $CO_2$ conversion into acetate.

## Coordination of "doped" acetogenesis and lipogenesis

Coordinating acetogenesis and lipogenesis allows $CO_2$-to-acetate-to-lipid conversion. Interestingly, the observed acetate and fatty acid productivities from glucose- and gluconate-doping ($V_{12}$) exceeded not only the measured productivities with individual substrates ($V_1$ or $V_2$) but also the expected productivity for the two substrates combined ($V_1 + V_2$) (**Fig. 6A**). The expected productivity was linearly extrapolated from the combination of supplemental glucose feeding with $CO_2$+$H_2$ batch fermentation for acetogenesis and the combination of supplemental gluconate feeding with acetate batch fermentation for lipogenesis (**Supplementary Information**).

We attributed the observed synergy ($V_{12}>V_1+V_2$) to complementary substrate cofeeding. While our $^{13}C$ labeling experiments showed the roles of glucose and gluconate in ATP and cofactor synthesis, respectively, we sought to define the theoretical framework that illustrates the feasibility of this synergy. To this end, stoichiometric analysis of the different fates of individual substrates was combined with experimentally measured rates of single-substrate acetogenesis and lipogenesis. The maximum carbon, ATP, and electron attainable with mixed substrates were then evaluated for the two processes (**Supplementary Information**). We identified that the ATP and NADPH generation by glucose and gluconate doping relieved the limiting ingredients for acetate and lipid synthesis, respectively, and, in conjunction with the primary substrates, better balanced the energy and cofactor ratio requirements for reduced bioproduct synthesis (**Fig. 6B**).

In terms of organic carbon yield, the integrated acetogenesis-lipogenesis process converted 1 g of glucose to ~13 g of lipids (0.154 g lipids/g acetate × ~82 g acetate/g glucose) by extensive $CO_2$

utilization. Increasing mass transfer rates of gases improves $H_2$ (and $CO_2$) utilization efficiency, and it has been reported that ~95% of supplied $H_2$ can be used by commercial $CO_2$-fixing microbes[30,31]. By continuously converting $CO_2$ and $H_2$ to lipids via coordinated acetogenesis and lipogenesis, 38% of energy from $H_2$ was stored as lipids and 14% as yeast biomass (**Fig. 6C**). Nearly all carbons (~99%) in lipids originated from $CO_2$.

To further explore the potential of our synergistic cofeeding approach, we applied the stoichiometric analysis to other acetyl-CoA derived products and determined the gains in productivities (**Fig. 6D and Supplementary Information**). Similar to the results for fatty acids, the model predicted synergy between the substrate pair in producing other reduced compounds such as polyhydroxybutyrate (PHB) and isopentenyl pyrophosphate (IPP, precursor for isoprenoids), leading to increases in productivities over the extrapolated sum ($V_{12}>V_1+V_2$). Therefore, our substrate cofeeding strategy may stimulate conversion of $CO_2$ into a wide array of advanced bioproducts.

## Discussion

One of the greatest biotechnological challenges is engineering metabolism. Current engineering efforts often focus on funneling metabolic fluxes through product synthesis pathways via assembling various gene pools and knocking out competing pathways with existing genetic tools[32]. In addition, most processes start from sugars as the sole substrate, which inherently causes some metabolic intermediates to be out of balance and surplus components to be wasted because of the differences in chemical properties between the substrate and the product. This further necessitates the use of genetic engineering for flux rewiring in order to achieve industrially relevant production metrics. Such approaches set a limit on the choice of microbial hosts based on genetic manipulability and the existing strategies are not generalizable to all organisms.

Here we presented the potential of mixed substrate cofeeding as a generalizable method and a more effective starting point for bioproduct synthesis. As the first step, we overcame the difficulties that arise due to organisms' preferential substrate usage. Controlled continuous feeding of a preferred substrate as a metabolic dopant did not inhibit the consumption of the less favored substrate. Using this approach, we enhanced the utilization of $CO_2$ and acetate, which are typically the end products of metabolism and therefore least preferred by organisms. This was demonstrated in both *M. thermacetica* and *Y. lipolytica*, two organisms with distinct metabolism and genetic manipulability, using various substrates (glucose and $H_2/CO_2$ as well as acetate and gluconate). Correspondingly, we expect this design to be widely applicable to other substrates and organisms.

Surprisingly, substrate cofeeding synergistically enhanced product synthesis. In both cases, the total product carbon flux resulting from co-utilized substrates ($V_{12}$) exceeded the sum of the individual substrate fluxes ($V_1 + V_2$). However, previous models describing substrate co-utilization have overlooked this synergistic effect[11]. The observation of $V_{12}>V_1 + V_2$ could be explained by the two substrates having distinct yet complementary functions in cellular metabolism. Our stoichiometric analysis of metabolic requirements and burdens suggested that glucose and gluconate as dopant substrates could indeed complement ATP and NADPH generation, alleviating the limitations seen in acetogenesis and lipogenesis, respectively. Importantly, the observed

significant enhancements in $CO_2$ and acetate reduction metabolism required only minor addition of "valuable" glucose and gluconate.

To understand how the dopant substrates can strikingly achieve such efficiency in enhancing reductive metabolism, we also elucidated the underlying mechanisms. Tracing $^{13}C$-labeled glucose and gluconate revealed that nearly all of these supplements went into ATP and NADPH production, respectively. We identified pyruvate kinase (PEP+ADP → Pyr+ATP) in *M. thermoacetica* and the pentose cycle (6PG → R5P → F6P → G6P → 6PG + 2 NADPH) in *Y. lipolytica* to be important cofactor generating steps. In particular, activating pyruvate kinase by cofeeding glucose solved the challenge of slow $CO_2$ fixation, which is due to ATP-limited metabolism in autotrophic fermentations[31,33]. Activating the pentose cycle by cofeeding gluconate solved the challenge of limited NADPH production through oxPPP in acetate-fed cells. Therefore, we rewired metabolism without genetic engineering by cofeeding dopant substrates.

Finally, akin to the widespread use of dopants in the electronics industry to enhance material properties, we envision the dopant substrate cofeeding scheme becoming valuable in a wide array of biotechnological applications. Our demonstration of $CO_2/H_2$-to-acetate-to-lipids conversion at high productivity and energetic efficiency serves as an exemplary renewable energy storage strategy using substrates that do not interfere with food supply. Since acetate is closely related to acetyl-CoA, a focal point in many metabolic pathways, other acetate-based processes applying proper doping substrates could enable rapid synthesis of a wide repertoire of bioproducts such as fatty acid derived oleochemicals[34] and mevalonate pathway derived natural products[35]. By coupling this to the glucose-doped acetogenesis, $CO_2$ could become the initial feedstock for all subsequent acetate-driven processes, benefiting both the environment and carbon economy. Moreover, the metabolic enhancements by cofeeding superior substrates is not limited to $CO_2$- and acetate-based fermentations. The imbalance of carbon building blocks, cofactors, and energy with respect to the desired product requirement can also be seen in many other single-substrate substrate bioconversions. In these cases, identification of complementary substrates and implementation of controlled dopant substrate cofeeding would optimally coordinate pathway usage for superior biosynthesis. Consequently, substrates previously considered infeasible for industrial bioprocesses due to limited productivity may become well-suited as economically and technologically viable feedstocks[36].

**Acknowledgments** The authors would like to thank Drs. Caroline Lewis and Elizaveta Freinkman for their help with LC-MS. This research was supported by U.S. Department of Energy grants DE-AR0000433, DE-SC0008744 and DE-SC0012377 as well as Mobility Plus Fellowship 1284/MOB/IV/2015/0.

**Author Contributions** J.O.P, N.L., and G.S. designed the study and wrote the paper. J.O.P., N.L. and K.M.H performed experiments and flux analysis. J.O.P., N.L., B.M.W., and C.V. developed LC-MS and GC-MS methods. J.O.P., N.L., D.F.E., J.X. designed the bioreactors. J.O.P. and M.A.I. developed the updated metabolic model. J.O.P., N.L., K.Q., Z.L., P.R.G. and G.S. analyzed the data.

## Figures

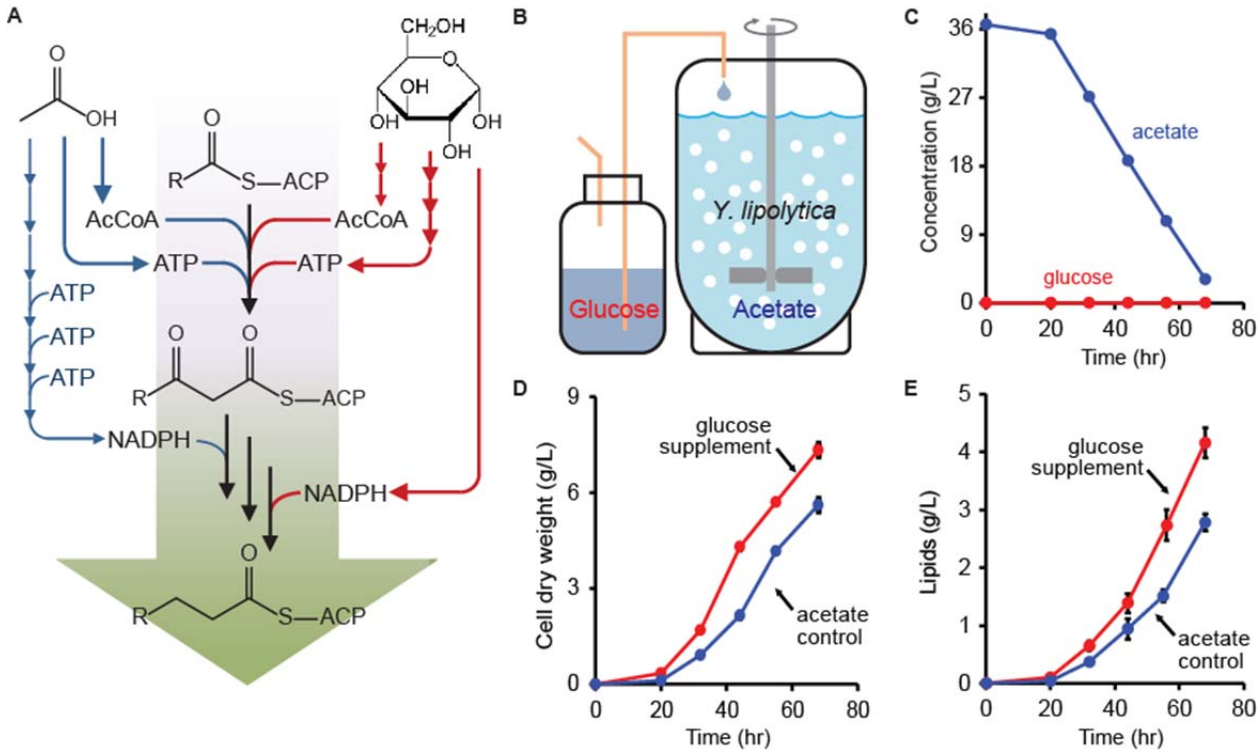


**Figure 1. Continuous glucose cofeeding relieves repression of acetate in *Y. lipolytica*.** (**A**) Acetate can efficiently support acetyl-CoA and ATP generation through the TCA cycle but not NADPH generation, which requires many enzymatic steps and ATP. Glucose, on the other hand, can produce NADPH more directly through oxPPP. (**B**) Since glucose batch feeding suppresses acetate consumption, glucose was continuously supplemented in small quantities to the acetate culture. (**C**) Despite the continuous feeding of glucose, its concentration in the reactor remained at 0 and acetate concentration decreased. Thus, the fed-batch system enabled simultaneous consumption of acetate and glucose. (**D**) Biomass and (**E**) lipid production was faster and higher with glucose-"doping" compared to the acetate-only control.

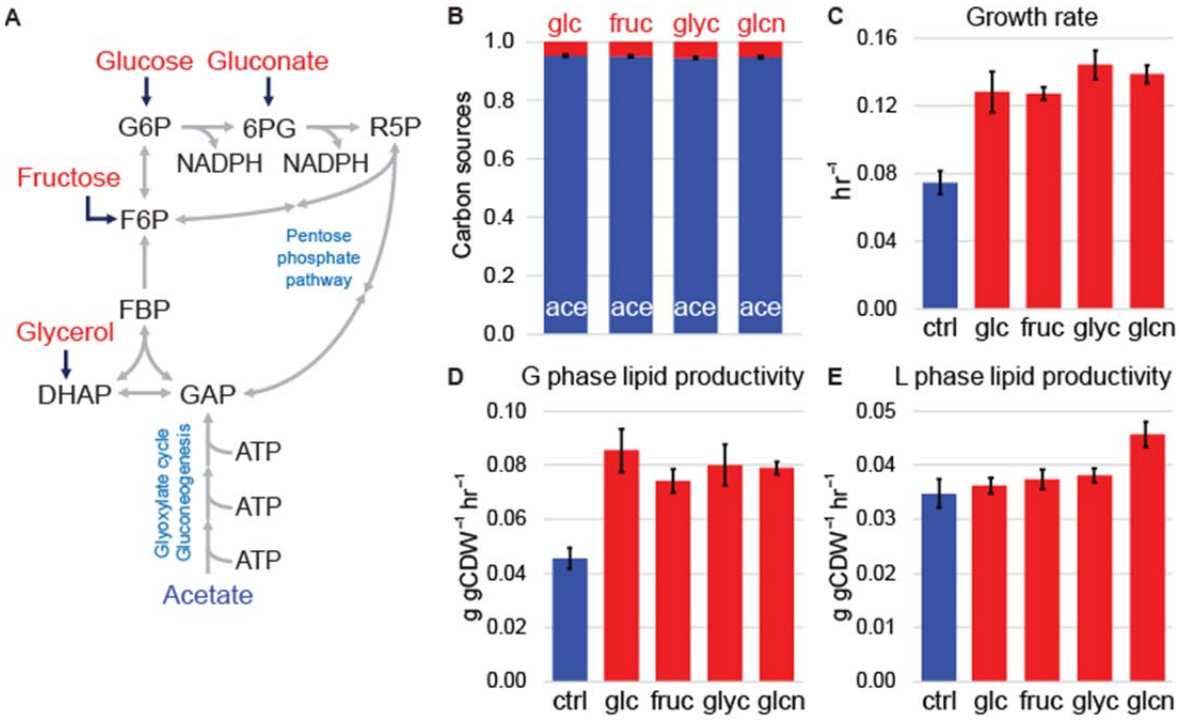


**Figure 2. Cofeeding substrates near oxidative pentose phosphate pathway accelerates cell growth and lipogenesis from acetate.** (**A**) Glucose, fructose, glycerol, and gluconate enter central carbon metabolism through upper glycolysis and PPP. (**B**) Supplementation of these four substrates accounted for ~5% of the total carbon consumed by the cells and the primary carbon source was acetate. (**C**) Specific growth rates nearly doubled with substrate cofeeding compared to the acetate-only control. (**D**) Growth phase (nitrogen-replete) specific lipid productivity nearly doubled with substrate cofeeding. (**E**) Lipogenic phase (nitrogen-depleted) specific lipid productivity was mildly enhanced by glucose, fructose, or glycerol supplementation. Gluconate-"doping" significantly outperformed the other conditions.

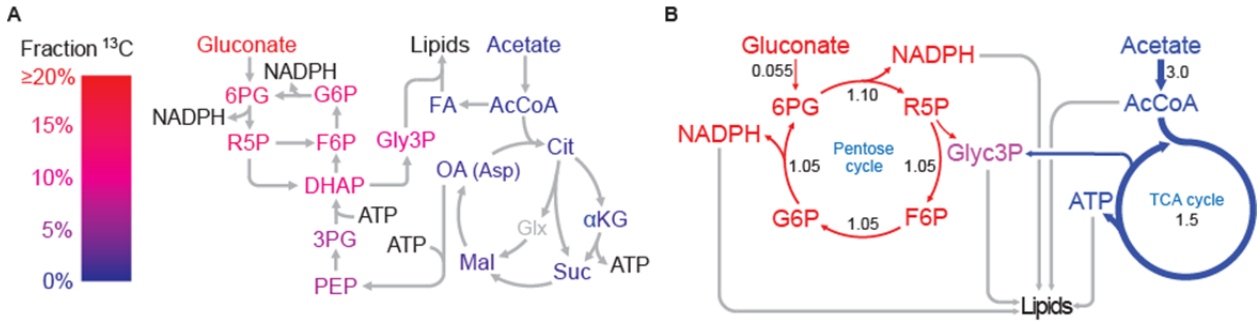


**Figure 3. Gluconate generates NADPH via the pentose cycle.** (**A**) Tracing carbons from [U-$^{13}C_6$]gluconate revealed partitioned usage of metabolism. The heavy $^{13}C$ of gluconate remained mainly in upper glycolysis and PPP. Acetyl-CoA and TCA intermediates were completely unlabeled, indicating exclusive contribution from acetate. (**B**) Metabolic flux analysis via isotope mass balancing revealed the cyclic reaction sequence generating NADPH. The "pentose cycle" consisted of the NADPH-producing oxPPP, transketolase, transaldolase, and phosphoglucose isomerase. Flux values are in mmol $gCDW^{-1}$ $hr^{-1}$.

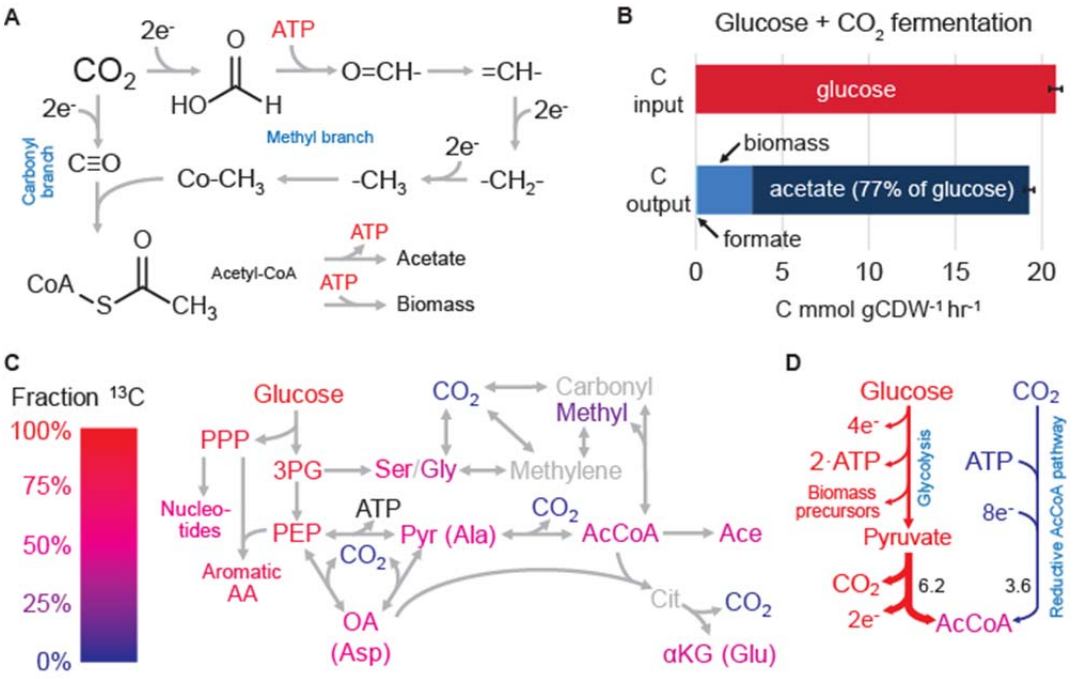


**Figure 4. Glucose generates ATP for $CO_2$ fixation but leads to decarboxylation in *M. thermoacetica*.** (**A**) The reductive acetyl-CoA pathway consists of the carbonyl and methyl branches for conversion of $CO_2$ into acetyl group. The methyl branch requires ATP. (**B**) Analysis of carbon input and output in batch cofeeding of *M. thermoacetica* with glucose and $CO_2$ revealed the preferential use of glucose. (**C**) Batch cofeeding [U-$^{13}C_6$]glucose and $CO_2$ revealed the simultaneous use of glucose and $CO_2$. Glucose carbons contributed mainly to glycolysis and PPP while partially to TCA cycle. A substantial fraction of TCA carbons was traced to $CO_2$. (**D**) Despite simultaneous utilization of $CO_2$, preferred glucose use led to undesirable decarboxylation outpacing $CO_2$ uptake. Flux values are in mmol $gCDW^{-1}$ $hr^{-1}$ of acetyl-CoA.

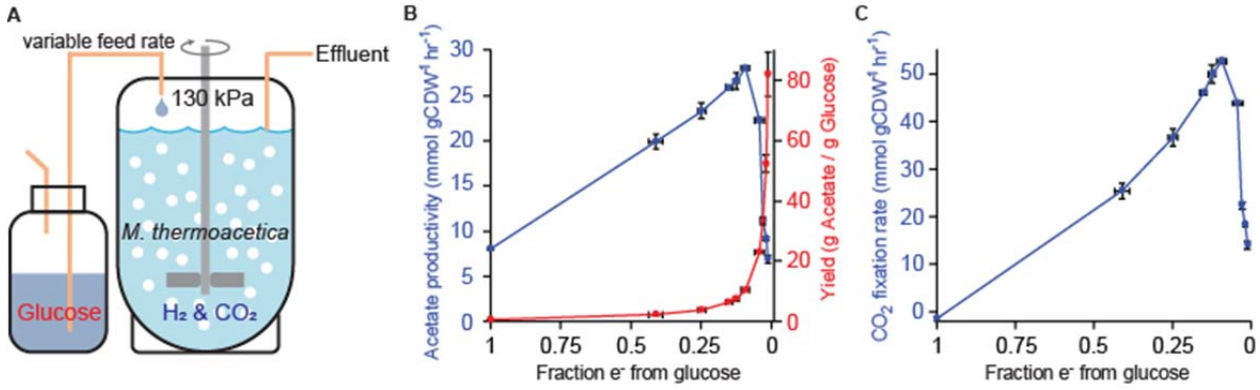


**Figure 5. Continuous glucose cofeeding accelerates acetogenesis from $CO_2$ fixation at the autotrophic limit.** (**A**) Since glucose batch feeding leads to undesirable decarboxylation, glucose was continuously supplemented in small quantities to gas-fermenting *M. thermoacetica* culture. (**B**,**C**) Acetate productivity, yield, and $CO_2$ fixation rate at varying ratios of electrons ($e^-$) derived from $H_2$ and glucose. The plots include both batch and chemostat data (**Supplementary Table 5**). (**B**) Acetate productivity peaked when 91% of $e^-$ were derived from $H_2$ and 9% glucose. On the other hand, carbon yield (acetate produced per glucose consumed) increased with increasing fraction of electrons from $H_2$. (**C**) $CO_2$ fixation rate peaked when 9% of $e^-$ were derived from glucose and remained high near the autotrophic limit.

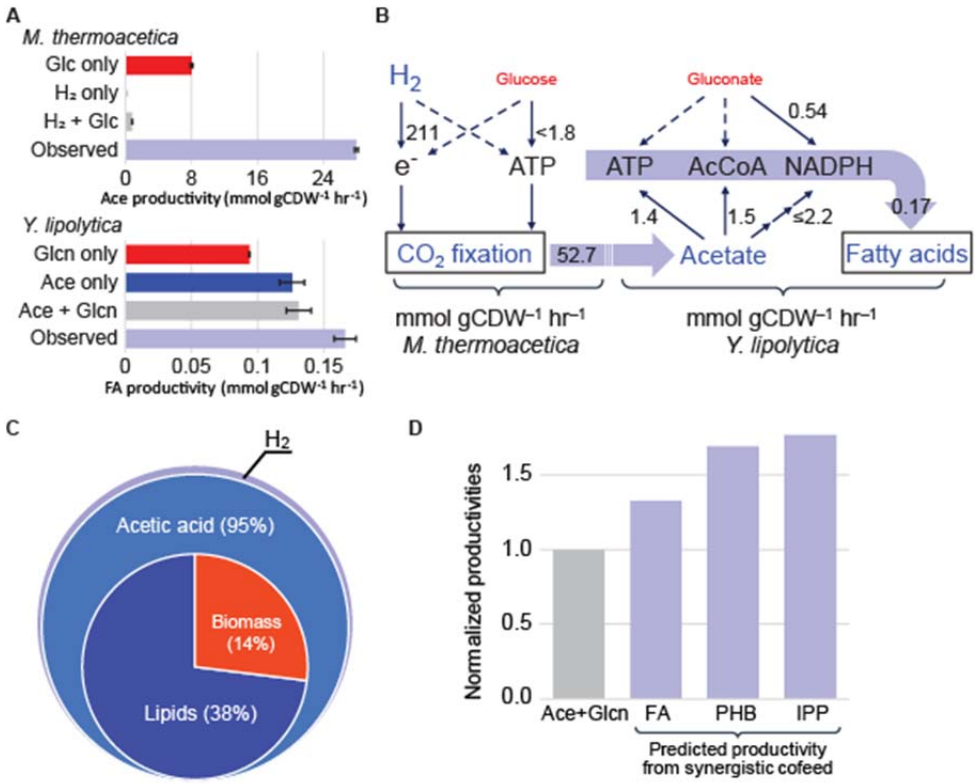


**Figure 6. Synergy and coordination of substrate cofeeding accelerate the conversion of $CO_2$ and $H_2$ into lipids.** (**A**) Glucose- and gluconate-doping resulted in synergy that accelerated acetogenesis and lipogenesis beyond the linear extrapolation of additional carbon supplement. (**B**) The maximum $CO_2$ fixation and fatty acid production rates were attained by cofeeding glucose and gluconate in limiting quantities. Stoichiometric analysis of metabolic requirements and burdens revealed the key role of glucose and gluconate in generating ATP and NADPH. The dashed arrows denote negligible contributions. (**C**) In terms of energy efficiency, 95% of $H_2$ energy can be stored as acetate by *M. thermoacetica* and 55% of acetate energy can be stored as lipids by *Y. lipolytica*. Coordination of acetogenesis and lipogenesis enabled storage of 38% of $H_2$ energy as lipids and 14% as biomass. (**D**) The cofeeding approach can also be applied to synthesizing other products with predicted synergistic productivity that exceeds the sum of individual-substrate productivities.

## References


1 Ledesma-Amaro, R. & Nicaud, J. M. Metabolic Engineering for Expanding the Substrate Range of Yarrowia lipolytica. *Trends Biotechnol* **34**, 798-809, doi:10.1016/j.tibtech.2016.04.010 (2016).

2 Atsumi, S., Hanai, T. & Liao, J. C. Non-fermentative pathways for synthesis of branched-chain higher alcohols as biofuels. *Nature* **451**, 86, doi:10.1038/nature06450 (2008).

3 Xue, Z. *et al.* Production of omega-3 eicosapentaenoic acid by metabolic engineering of Yarrowia lipolytica. *Nat Biotechnol* **31**, 734-740, doi:10.1038/nbt.2622 (2013).

4 Qiao, K. J., Wasylenko, T. M., Zhou, K., Xu, P. & Stephanopoulos, G. Lipid production in Yarrowia lipolytica is maximized by engineering cytosolic redox metabolism. *Nature biotechnology* **35**, 173-177, doi:10.1038/nbt.3763 (2017).

5 Kita, A. *et al.* Development of genetic transformation and heterologous expression system in carboxydotrophic thermophilic acetogen Moorella thermoacetica. *J Biosci Bioeng* **115**, 347-352, doi:10.1016/j.jbiosc.2012.10.013 (2013).

6 Monod, J. Recherches sur la croissance des cultures bacteriennes. (1942).

7 Aristilde, L., Lewis, I. A., Park, J. O. & Rabinowitz, J. D. Hierarchy in Pentose Sugar Metabolism in Clostridium Acetobutylicum. *Appl Environ Microbiol*, doi:10.1128/AEM.03199-14 (2014).

8 Goerke, B. & Stulke, J. Carbon catabolite repression in bacteria: many ways to make the most out of nutrients. *Nat Rev Microbiol* **6**, 613-624, doi:Doi 10.1038/Nrmicro1932 (2008).

9 Bren, A. *et al.* Glucose becomes one of the worst carbon sources for E.coli on poor nitrogen sources due to suboptimal levels of cAMP. *Sci Rep* **6**, 24834, doi:10.1038/srep24834 (2016).

10 Joshua, C. J., Dahl, R., Benke, P. I. & Keasling, J. D. Absence of diauxie during simultaneous utilization of glucose and Xylose by Sulfolobus acidocaldarius. *J Bacteriol* **193**, 1293-1301, doi:10.1128/JB.01219-10 (2011).

11 Hermsen, R., Okano, H., You, C., Werner, N. & Hwa, T. A growth-rate composition formula for the growth of E.coli on co-utilized carbon substrates. *Mol Syst Biol* **11**, 801, doi:10.15252/msb.20145537 (2015).

12 Kanno, M., Carroll, A. L. & Atsumi, S. Global metabolic rewiring for improved CO2 fixation and chemical production in cyanobacteria. *Nature communications* **8**, doi:10.1038/Ncomms14724 (2017).

13 Martinez, K. *et al.* Coutilization of glucose and glycerol enhances the production of aromatic compounds in an Escherichia coli strain lacking the phosphoenolpyruvate: carbohydrate phosphotransferase system. *Microb Cell Fact* **7**, 1, doi:10.1186/1475-2859-7-1 (2008).

14 Meyer, F. *et al.* Methanol-essential growth of Escherichia coli. *Nature communications* **9**, doi:10.1038/S41467-018-03937-Y (2018).

15 Garcia Sanchez, R. *et al.* Improved xylose and arabinose utilization by an industrial recombinant Saccharomyces cerevisiae strain using evolutionary engineering. *Biotechnol Biofuels* **3**, 13, doi:10.1186/1754-6834-3-13 (2010).

16 Kim, S. M. *et al.* Simultaneous utilization of glucose and xylose via novel mechanisms in engineered Escherichia coli. *Metab Eng* **30**, 141-148, doi:10.1016/j.ymben.2015.05.002 (2015).

17 Jones, S. W. *et al.* CO2 fixation by anaerobic non-photosynthetic mixotrophy for improved carbon conversion. *Nat Commun* **7**, 12800, doi:10.1038/ncomms12800 (2016).
18 Bowes, G., Hageman, R. H. & Ogren, W. L. Light Saturation, Photosynthesis Rate, Rudp Carboxylase Activity, and Specific Leaf Weight in Soybeans Grown under Different Light Intensities. *Crop Sci* **12**, 77-& (1972).
19 Xu, J., Liu, N., Qiao, K., Vogg, S. & Stephanopoulos, G. Application of metabolic controls for the maximization of lipid production in semicontinuous fermentation. *Proc Natl Acad Sci U S A* **114**, E5308-E5316, doi:10.1073/pnas.1703321114 (2017).
20 Ratledge, C. & Wynn, J. P. The biochemistry and molecular biology of lipid accumulation in oleaginous microorganisms. *Advances in applied microbiology* **51**, 1-51 (2002).
21 Qiao, K. *et al.* Engineering lipid overproduction in the oleaginous yeast Yarrowia lipolytica. *Metab Eng* **29**, 56-65, doi:10.1016/j.ymben.2015.02.005 (2015).
22 Fontanille, P., Kumar, V., Christophe, G., Nouaille, R. & Larroche, C. Bioconversion of volatile fatty acids into lipids by the oleaginous yeast Yarrowia lipolytica. *Bioresource Technology* **114**, 443-449, doi:https://doi.org/10.1016/j.biortech.2012.02.091 (2012).
23 Liu, N., Qiao, K. & Stephanopoulos, G. (13)C Metabolic Flux Analysis of acetate conversion to lipids by Yarrowia lipolytica. *Metab Eng* **38**, 86-97, doi:10.1016/j.ymben.2016.06.006 (2016).
24 Gancedo, J. M. Carbon catabolite repression in yeast. *Eur J Biochem* **206**, 297-313 (1992).
25 Casazza, J. P. & Veech, R. L. The Interdependence of Glycolytic and Pentose Cycle Intermediates in Ad-Libitum Fed Rats. *J Biol Chem* **261**, 690-698 (1986).
26 Ragsdale, S. W. & Pierce, E. Acetogenesis and the Wood-Ljungdahl pathway of CO(2) fixation. *Biochimica et biophysica acta* **1784**, 1873-1898, doi:10.1016/j.bbapap.2008.08.012 (2008).
27 Mall, A. *et al.* Reversibility of citrate synthase allows autotrophic growth of a thermophilic bacterium. *Science* **359**, 563-567, doi:10.1126/science.aao2410 (2018).
28 Nunoura, T. *et al.* A primordial and reversible TCA cycle in a facultatively chemolithoautotrophic thermophile. *Science* **359**, 559-563, doi:10.1126/science.aao3407 (2018).
29 Schuchmann, K. & Muller, V. Autotrophy at the thermodynamic limit of life: a model for energy conservation in acetogenic bacteria. *Nat Rev Microbiol* **12**, 809-821, doi:10.1038/nrmicro3365 (2014).
30 Daniell, J., Köpke, M. & Simpson, S. Commercial Biomass Syngas Fermentation. *Energies* **5**, 5372 (2012).
31 Hu, P., Rismani-Yazdi, H. & Stephanopoulos, G. Anaerobic CO2 fixation by the acetogenic bacterium Moorella thermoacetica. *AIChE Journal* **59**, 3176-3183, doi:10.1002/aic.14127 (2013).
32 Blazeck, J. *et al.* Harnessing Yarrowia lipolytica lipogenesis to create a platform for lipid and biofuel production. *Nat Commun* **5**, 3131, doi:10.1038/ncomms4131 (2014).
33 Daniel, S. L., Hsu, T., Dean, S. I. & Drake, H. L. Characterization of the H2- and CO-dependent chemolithotrophic potentials of the acetogens Clostridium thermoaceticum and Acetogenium kivui. *J Bacteriol* **172**, 4464-4471 (1990).

34 Ledesma-Amaro, R., Dulermo, R., Niehus, X. & Nicaud, J. M. Combining metabolic engineering and process optimization to improve production and secretion of fatty acids. *Metab Eng* **38**, 38-46, doi:10.1016/j.ymben.2016.06.004 (2016).
35 Martin, V. J. J., Pitera, D. J., Withers, S. T., Newman, J. D. & Keasling, J. D. Engineering a mevalonate pathway in Escherichia coli for production of terpenoids. *Nature biotechnology* **21**, 796-802, doi:10.1038/nbt833 (2003).
36 Haynes, C. A. & Gonzalez, R. Rethinking biological activation of methane and conversion to liquid fuels. *Nat Chem Biol* **10**, 331-339, doi:10.1038/nchembio.1509 (2014).

## Methods

### Strains and culture conditions

*Yarrowia lipolytica* strains based on the ACCDGA strain (MTYL065)[37] were pre-cultured at 30 °C in 14 mL test tubes containing YPD media (20 g/L glucose, 20 g/L peptone, 10 g/L yeast extract). After 24 hr, 1 mL culture was transferred to a shake flask containing 40 mL of acetate media (50 g/L sodium acetate, 1.7 g/L YNB-AA-AS, and 1.34 g/L ammonium sulfate). The shake flask culture was carried out for 24 hr to adapt the cells to acetate. Afterwards, the cells were pelleted at 18,000 g for 5 min, washed once with acetate media, and used for inoculation at an initial $OD_{600}$ of 0.05 for all *Y. lipolytica* experiments.

Mixed substrate batch cultures were carried out in shake flasks with 40 mL of acetate media except that 6 mol% of the total carbon from acetate was replaced with the supplemental substrate (glucose, fructose, glycerol, or gluconate). Continuous fed-batch supplementation cultures were carried out in 250 mL bioreactors (Applikon Biotechnology) with 150 mL working volume. Acetate media was used under batch conditions while the supplemented substrate was continuously fed at a rate of 0.13 mmol C/hr. For the acetate-only control case, the supplemented substrate was replaced with acetate and fed at the same rate to ensure that cells had equal amounts of carbon substrates throughout all conditions. All bioreactor cultures were carried out at 30 °C, pH 7.0 (controlled with 10 wt% sulfuric acid), and 0.2 LPM air sparging. The dissolved oxygen levels were controlled at 20% during the growth phase and ~2% during the lipogenic phase for optimal lipid production and minimal citrate excretion[4]. For gluconate $^{13}C$ tracing experiments, natural gluconate in the supplementation feed stream was replaced with [U-$^{13}C_6$]gluconate (99%, Cambridge Isotope Laboratories).

In all *Y. lipolytica* experiments having gluconate as a substrate, an ACCDGA strain overexpressing its native gluconate kinase (glucK) under the *TEFin* promoter was used. The expression of *TEFin*-glucK was performed through genome integration. This was to ensure that gluconate uptake and incorporation into central carbon metabolism was not inhibited by inadequate levels of the kinase. All other experiments were performed using the same ACCDGA strain with an empty control vector

integrated into the genome. Overexpressing gluconate kinase did not have any appreciable effects on the strain's capability to produce lipids on acetate, as shown in **Supplementary Fig. 9**.

*Moorella thermoacetica* (ATCC 39073 and 49707) were cultured in balch-type tubes containing culture medium with 8 g/L glucose, 7.5 g/L $NaHCO_3$, 7 g/L $KH_2PO_4$, 5.5 g/L $K_2HPO_4$, 2 g/L $(NH_4)_2SO_4$, 0.5 g/L $MgSO_4 \bullet 7H_2O$, 0.3 g/L cysteine, 0.02 g/L $CaCl_2 \bullet 2H_2O$, 1% (v/v) trace minerals (ATCC MD-TMS), and 1% (v/v) vitamins (ATCC MD-VS) at 55 °C pH 6.8. Cysteine scavenged residual dissolved oxygen in the medium[38]. The headspace was pressurized to either 170 kPa with $CO_2$ or 240 kPa with 80:20 $H_2/CO_2$. For $^{13}C$ tracing experiments, natural glucose was replaced with [U-$^{13}C_6$]glucose (99%, Cambridge Isotope Laboratories) and the headspace was pressurized to 170 kPa with natural $CO_2$. The balch-tube cultures were incubated inside a strictly anoxic glovebox with magnetic stirring.

For bioreactor experiments, *M. thermoacetica* (ATCC 49707) was cultured in a strictly anoxic vessel with pH and temperature control set to 6.6 (using 10M sodium hydroxide) and 55°C. Low glucose but otherwise identical culture media were fed as follows (media glucose concentrations and media feed rates): 0.25 g/L at 11.5 mL/hr; 0.25 g/L at 9.1 mL/hr; 0.25 g/L at 6.9 mL/hr; 0.25 g/L at 4.3 mL/hr; 0.25 g/L at 2.3 mL/hr; 0.25 g/L at 1.2 mL/hr; and 0.13 g/L at 1.2 mL/hr. The rate of effluent was the same to keep the culture volume constant at 135 mL. $H_2$ and $CO_2$ were mixed at 60:40 and sparged into the culture at 200 mL/min. The headspace pressure was maintained at 130 kPa. All the data and conditions are shown in **Supplementary Table 5**.

**Metabolite extraction and measurement**

To extract metabolites, *Y. lipolytica* cells were collected during exponential and lipogenic phases. Cells were filtered on 0.45 μm nylon membrane filters and immediately transferred to a precooled 40:40:20 acetonitrile/methanol/water solution. After 20 minutes at -20°C, the filters were washed, and extracts were moved to Eppendorf tubes. The samples were then centrifuged for five minutes and the supernatants were dried under nitrogen.

In mid-exponential phase, the *M. thermoacetica* cultures were collected from balch-type tubes using syringes inside the anaerobic glovebox. Immediately after, cellular metabolism was quenched and metabolites were extracted by quickly transferring filtered cells (on 0.2 μm nylon membrane filter) to plates containing precooled 80% acetonitrile on ice[39]. After 20 minutes at 4°C, the membrane filters were washed, and the metabolite extracts were moved to Eppendorf tubes. The supernatants were obtained after five minutes of centrifugation and lyophilized.

Dried samples were resuspended in HPLC-grade water for LC-MS analysis. These samples were analyzed on a Dionex UltiMate 3000 UPLC system (Thermo) with a ZIC-pHILIC (5 μm polymer particle) 150 × 2.1 mm column (EMD Millipore) coupled to a QExactive orbitrap mass spectrometer (Thermo) by electrospray ionization. With 20 mM ammonium carbonate, 0.1% ammonium hydroxide as solvent A and acetonitrile as solvent B, the chromatographic gradient was run at a flow rate of 0.150 mL/min as a linear gradient from 80% B to 20% B between 0 and 20 mins, a linear gradient from 20% B to 80% B between 20 and 20.5 mins, and 80% B held from 20.5 to 28 mins. The column and autosampler tray temperature were at 25 °C and 4 °C. The mass spectrometer was operated in polarity switching mode scanning a range of 70-1,000 m/z. The

resolving power was set to 70,000 for $^{13}C$ labeling experiments. With retention times determined by authenticated standards, resulting mass spectra and chromatograms were identified and processed using MAVEN software[40]. To obtain labeling information of cellular bicarbonate and acetate, the labeling of carbamoyl group was obtained by comparing (i.e., computing the inverse Cauchy product) citrulline to ornithine, and the labeling of acetyl group was obtained by comparing N-acetyl-glutamate to glutamate.

**Substrate uptake and product secretion measurement**

For *Y. lipolytica*, 1 mL of culture was taken at each time point for media and cell dry weight (CDW) analysis. The cells were centrifuged at 18,000 g for 10 min and the supernatant was subsequently extracted, filtered (0.2 μm syringe filters), and analyzed on a high-performance liquid chromatography (HPLC). The cell pellet was then wash once with 1 mL water to remove residual media components and dried in a 60 °C oven until its mass remains unchanged. This mass was taken to be the CDW per mL of culture. As for lipids, a small volume was extracted from the culture such that it contains ~1 mg of CDW. The supernatant was discarded after centrifugation at 18,000g for 10 min. 100 μL of an internal standard containing 2 mg/mL methyl tridecanoate (Sigma-Aldrich) and 2 mg/mL glyceryl triheptadecanoate (Sigma-Aldrich) in hexane was added to each sample. Transesterification was then carried out in 500 μL 0.5 N sodium methoxide solutions with continuous vortexing at 1200 rpm for 60 min. Afterwards, 40 μL of 98% sulfuric acid was added to neutralize the pH and 500 μL of hexane was used for extraction. Additional vortexing at 1200 rpm for 30 min was carried out and centrifugation at 6,000 g for 1 min was performed to remove cellular debris. The top hexane layer was used for analysis on a GC-FID system. All *Y. lipolytica* specific rate data were normalized to the lipid-free CDW, which was the difference between the measured CDW and the lipid titer.

For media analysis in *M. thermoacetica* cultures, small aliquots of the cultures were collected with syringes inside the anaerobic glovebox over their exponential phase. Filtered media samples (0.2 μm syringe filters) were analyzed by YSI biochemistry analyzer for glucose and by HPLC for acetate and formate along with other potential products (e.g., lactate and ethanol). Culture density was measured by spectrophotometry (0.45 gCDW $L^{-1}$ $OD_{660}^{-1}$) at the time of sampling. The rates of substrate uptake and product secretion were determined using the rates at which substrates, products, culture density change over time. The carbon output rate for biomass was determined using growth rate and elemental biomass composition of $CH_{2.08}O_{0.53}N_{0.24}$ [41]. The net $CO_2$ fixation rates were calculated based on the measured acetate and biomass carbon production rates less the corresponding measured glucose carbon consumption rates. The fraction of electrons derived from $H_2$ was inferred from the fraction of acetate and biomass carbons generated from net $CO_2$ fixation since the average oxidation state of acetate and biomass carbons is nearly the same as that of glucose.

For HPLC, 10 μL sample was injected into an Agilent 1200 High-Performance Liquid Chromatography system coupled to a G1362 Refractive Index Detector (Agilent Technologies). A Bio-Rad HPX-87H column was used for separation with 14 mM sulfuric acid as the mobile phase flowing at 0.7 mL/min. For GC-FID, 1 μL of sample was injected at a split ratio of 50:1 into an Agilent 7890B GC-FID system coupled to a J&W HP-INNOWax capillary column (Agilent

Technologies). The column was held at a constant temperature of 200 °C with helium as the carrier gas (1.5 mL/min). The injection and FID temperatures were set to 260 °C.

**Headspace gas measurement**

After collecting the *M. thermoacetica* cultures from balch-type tubes inside the anaerobic glovebox for intracellular and extracellular metabolite analysis, the empty balch-type tubes containing only the headspace gas were stored at 4 °C until gas chromatography-mass spectrometry (GC-MS) analysis. To measure $CO_2$ isotope labeling, 100 µl of headspace sample was collected from each tube with a gastight syringe and injected in a multimode inlet, which was maintained at 180 °C, with a split of 10. Samples were analyzed on a 7890A GC system with a 60 m GS-GasPro (0.320 mm diameter) column coupled with a 5975C quadrupole mass spectrometer (Agilent). The oven was kept at 90 °C for 3 minutes before heating to 260 °C at 45 °C/min and held at 260 °C for 1 minute.

**Flux balance analysis and isotope tracing flux analysis**

*M. thermoacetica* model based on the published genome-scale metabolic reconstruction[42] was employed for constraint-based flux analysis (see **Supplementary Information**). Among the feasible metabolic flux distributions that satisfy steady-state mass balance and nutrient availability constraints, optimal solutions that maximize/minimize objective functions were obtained using the COBRA toolbox and a Gurobi solver[43]. To determine $CO_2$ utilization capability, the objective was to maximize $CO_2$ consumption, or equivalently, minimize $CO_2$ production. To determine the growth potential using $H_2$ as the energy source, the objective was to maximize biomass production (i.e., cell growth). Substrate uptake and product secretion rate constraints were selected based on experimental or previously reported values.

To determine flux distributions, isotopomer mass balance constraints were also imposed based on the $^{13}C$ labeling results. For this purpose, the metabolic networks including glycolysis and PPP for *Y. lipolytica* as well as lower glycolysis, the TCA cycle, anaplerosis, the reductive acetyl-CoA pathway and the serine/glycine pathway for *M. thermoacetica* were constructed with carbon atom mapping. The labeling of following metabolites were simulated by the elementary metabolite unit (EMU) framework[44]: for *Y. lipolytica*, G6P, F6P, 3PG, S7P, 6PG, R5P, PEP, and Pyr (**Supplementary Table 1**); for *M. thermoacetica*, 3PG, PEP, Ala, acetyl-CoA, Ser, Gly, Asp, Glu, and $CO_2$ (**Supplementary Table 3**).

The flux distribution that best simulated the metabolite labeling and uptake-secretion rates was found by minimizing the variance weighted-sum of squared residuals (SSR) between simulation and experiment:

$$\min_{v} \sum \left( \frac{iso_{exp} - iso(v)}{s_{iso}} \right)^2 + \sum \left( \frac{v_{exp} - v}{s_v} \right)^2$$

$v$ and $iso(v)$ denote in vector form the metabolic flux distribution and the simulated $^{13}C$ labeling of metabolites as a function of $v$. $v_{exp}$ and $iso_{exp}$ denote measured fluxes and measured metabolite labeling; $s_v$and $s_{iso}$, their measurement standard deviation. The 95% confidence interval for each best fit flux was obtained by searching for the minimum and maximum flux values that increase the minimum SSR by less than the $\chi^2$ cutoff (1 degree of freedom) of 3.84.[45]

## Code availability

The code for metabolic flux and free energy analysis is available on the GitHub public repository: https://github.com/jopark/moorella_yarrowia

## References


37 Tai, M. & Stephanopoulos, G. Engineering the push and pull of lipid biosynthesis in oleaginous yeast Yarrowia lipolytica for biofuel production. *Metab Eng* **15**, 1-9, doi:10.1016/j.ymben.2012.08.007 (2013).

38 Michaelis, L. & Barron, E. S. G. Oxidation-reduction systems of biological significance. II. Reducing effect of cysteine induced by free metals. *J Biol Chem* **81**, 29-40 (1929).

39 Rabinowitz, J. D. & Kimball, E. Acidic acetonitrile for cellular metabolome extraction from Escherichia coli. *Anal Chem* **79**, 6167-6173, doi:Doi 10.1021/Ac070470c (2007).

40 Clasquin, M. F., Melamud, E. & Rabinowitz, J. D. LC-MS data processing with MAVEN: a metabolomic analysis and visualization engine. *Current protocols in bioinformatics / editoral board, Andreas D. Baxevanis ... [et al.]* **Chapter 14**, Unit14 11, doi:10.1002/0471250953.bi1411s37 (2012).

41 Tracy, B. P., Jones, S. W., Fast, A. G., Indurthi, D. C. & Papoutsakis, E. T. Clostridia: the importance of their exceptional substrate and metabolite diversity for biofuel and biorefinery applications. *Curr Opin Biotech* **23**, 364-381, doi:10.1016/j.copbio.2011.10.008 (2012).

42 Islam, M. A., Zengler, K., Edwards, E. A., Mahadevan, R. & Stephanopoulos, G. Investigating Moorella thermoacetica metabolism with a genome-scale constraint-based metabolic model. *Integr Biol (Camb)* **7**, 869-882, doi:10.1039/c5ib00095e (2015).

43 Schellenberger, J. *et al.* Quantitative prediction of cellular metabolism with constraint-based models: the COBRA Toolbox v2.0. *Nat Protoc* **6**, 1290-1307, doi:10.1038/nprot.2011.308 (2011).

44 Antoniewicz, M. R., Kelleher, J. K. & Stephanopoulos, G. Elementary metabolite units (EMU): A novel framework for modeling isotopic distributions. *Metab Eng* **9**, 68-86, doi:Doi 10.1016/J.Ymben.2006.09.001 (2007).

45 Antoniewicz, M. R., Kelleher, J. K. & Stephanopoulos, G. Determination of confidence intervals of metabolic fluxes estimated from stable isotope measurements. *Metab Eng* **8**, 324-337, doi:Doi 10.1016/J.Ymben.2006.01.004 (2006).